Structure and Unfolding of the Third Type III Domain from Human Fibronectin

Jessica M. Stine, Yizhi Sun, Geoffrey Armstrong, Bruce E. Bowler, and Klára Briknarová

Presentation Structure

Introduction
Objectives
Experimental Procedures
Results
Overall Findings

Introduction

What is Fibronectin?

What are the roles of Fibronectin?

Adhesion
Migration
Proliferation
Survival
Differentiation
Tissue repair

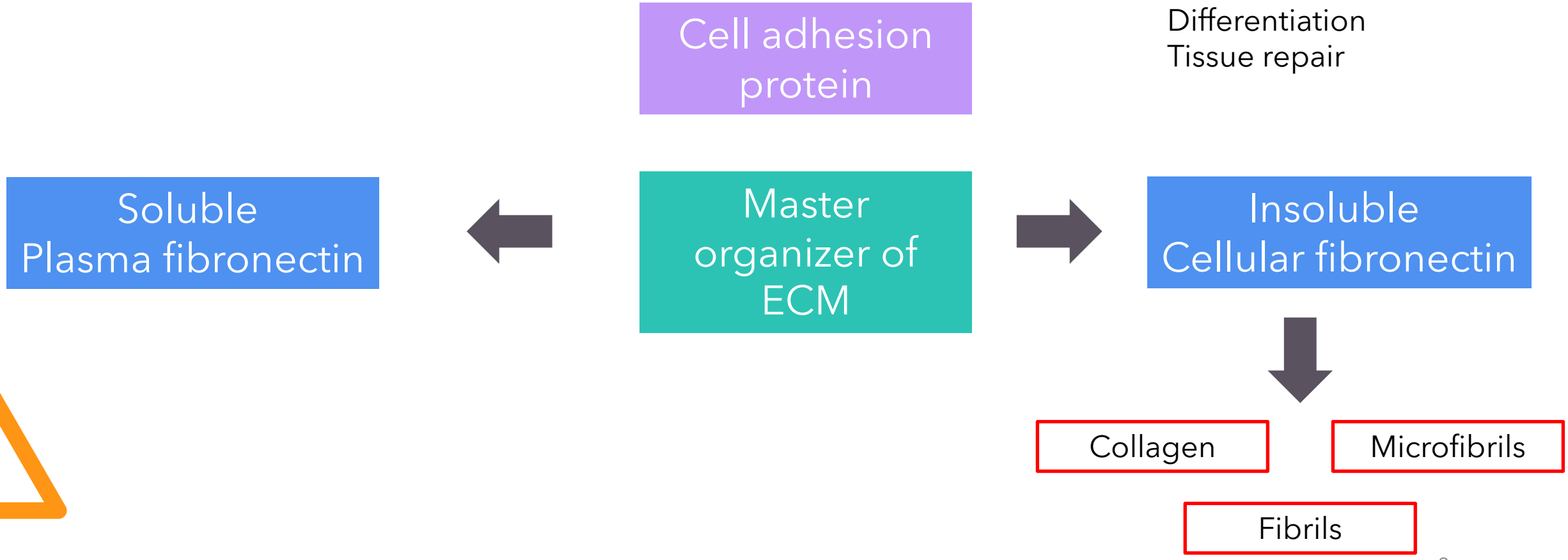

Introduction

What is the structure of Fibronectin?

3 types of homologous repeats
type 1 (FN1)
type 2 (FN2)
type 3 (FN3)

12x FN1
2x FN2
17x FN3

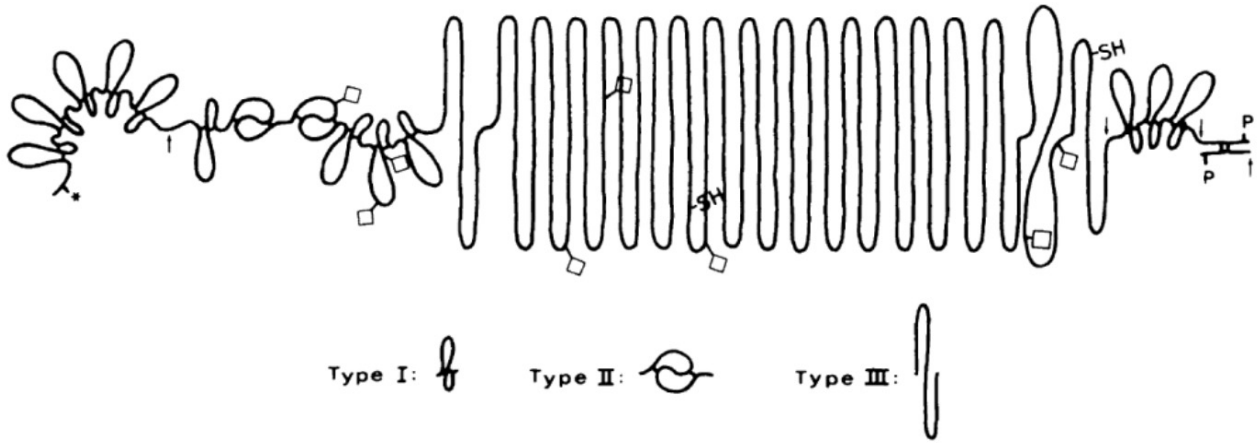

Mosher, D. F. (1989) Fibronectin, Academic Press, New York.

3FN3

Anastellin

Introduction

- What is Anastellin?

Carboxy-terminal fragment of the **first FN3 (type 3)** domain of Fibonectin.

Properties of Anastellin in the cell:
Anti-tumor
Anti-metastatic
Anti-angiogenic

- Role of Anastellin with 3FN3

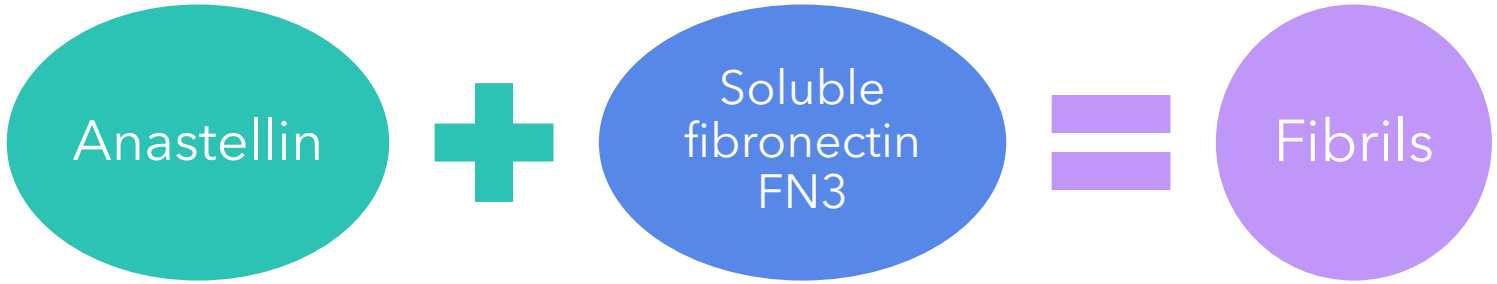

? HOW and WHY

Transient opening of FN3 domain = Anastellin binding

Presentation Structure

Introduction

Objectives

Experimental Procedures

Results

Overall Findings

Objectives

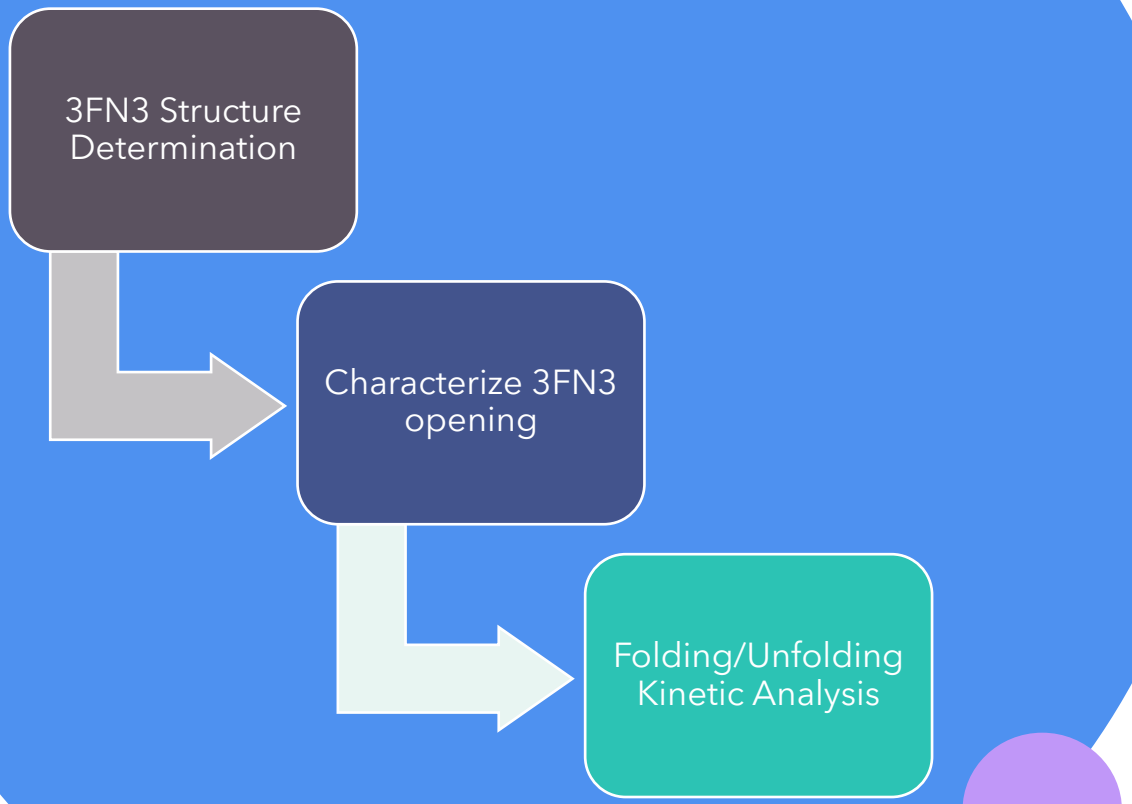
3FN3 Structure Determination
Characterize 3FN3 opening
Folding/Unfolding Kinetic Analysis

Presentation Structure

Introduction

Objectives

Experimental Procedures

Results

Overall Findings

Experimental Procedures

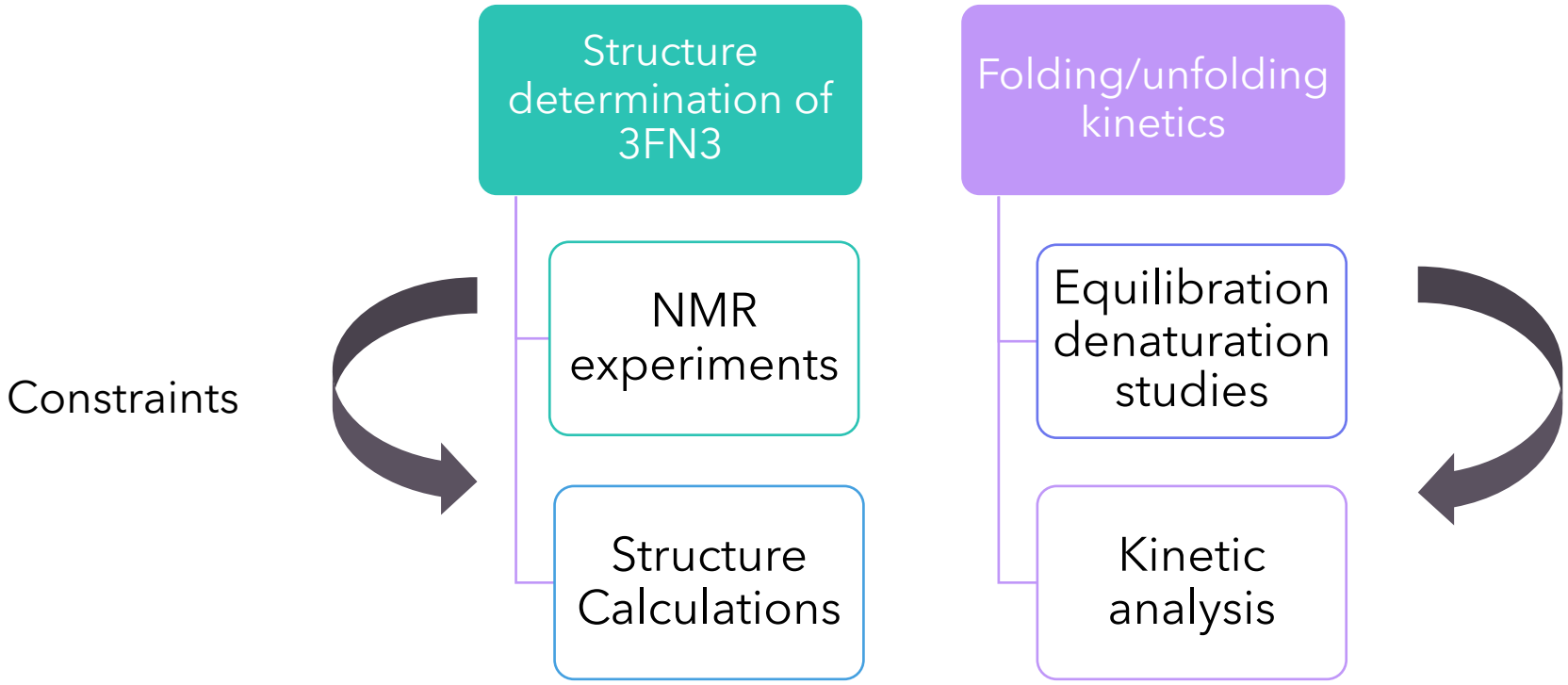

Experimental Procedures

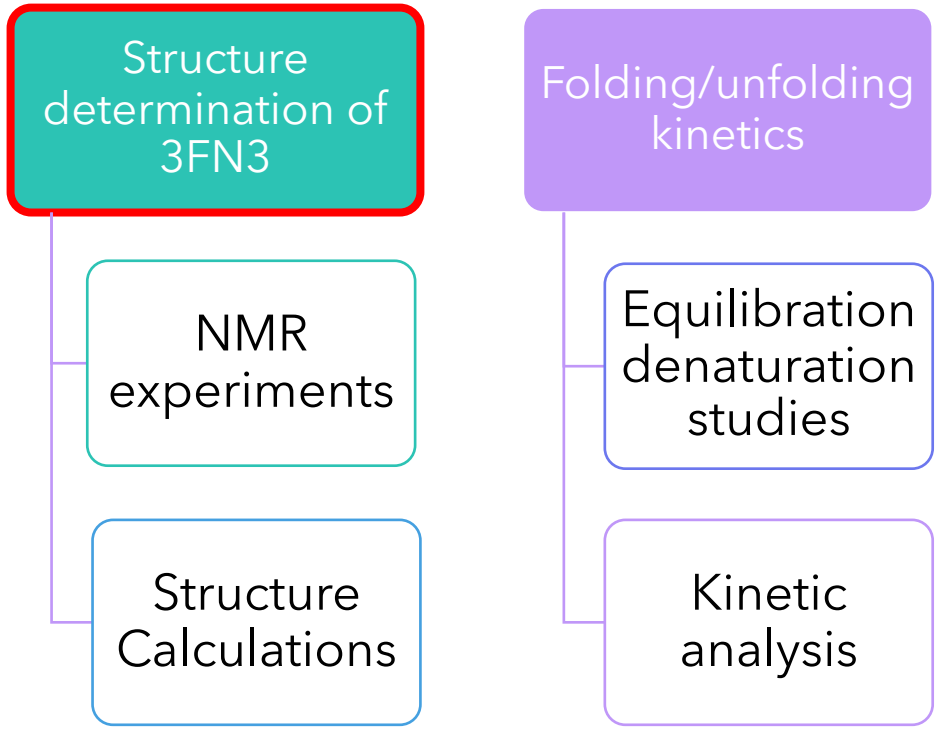

Experimental Procedures

- NMR Spectroscopy

Varian 600MHz or 800MHz NMR System at 25°C with a triple-resonance probe or a ^{13}C-enhanced salt-tolerant cold probe.

0.6 mM 3FN3
- Unlabeled
- ^{15}N Labelled
- ^{13}C and ^{15}N labeled

In PBS with 10% $^{2}H2O$

0.09 mM 3FN3
- Unlabeled
- 15N labeled
- ^{13}C and ^{15}N labeled

In PBS with 10% $^{2}H2O$

2D NMR

- ^{1}H-^{15}N HSQC
- ^{1}H-^{15}N HMQC
- ^{1}H-^{13}C aliphatic and aromatic HSQC
- COSY
- TOCOSY
- NOESY
- HBCB(CGCD)HD
- HMQC
- ^{13}C and ^{15}C filtered NOESY
- ^{13}C and ^{15}C edited NOESY

3D NMR

- HNCACB
- CBCA(CO)NH
- C(CO)NH
- H(CCO)NH
- HNCO
- HN(CA)CO
- CCH-TOCSY
- HCCH-TOCSY
- ^{15}N-edited TOCSY
- ^{15}N-edited NOESY
- ^{13}C-edited aliphatic and aromatic NOESY

Presentation Structure

Introduction

Objectives

Experimental Procedures

Results

Overall Findings

Results

Table 1. Experimental Restraints and Structural Statistics for 3FN3

no. of peaks in NOESY spectra	
3D ^{15}N-edited NOESY	1057
3D ^{13}C-edited aliphatic NOESY (without sensitivity enhancement)	1722
3D ^{13}C-edited aliphatic NOESY (sensitivity-enhanced)	906
3D ^{13}C-edited aromatic NOESY	64
2D NOESY in H_2O	1912
2D NOESY in D_2O	1343
2D ^{13}C- and ^{15}N-filtered, ^{13}C- and ^{15}N-edited NOESY	25
no. of experimental restraints	
NOE distance restraints in the last ARIA iteration	
intraresidual	873
sequential	454
medium-range ($2 \leq \|i - j\| \leq 5$)	171
long-range ($6 \leq \|i - j\|$)	758
ambiguous	1179
dihedral angle (Φ and Ψ)	168
hydrogen bond distance	60
no. of experimental restraint violations	
distance (NOE and hydrogen bond) violations >0.5 Å	0.2 ± 0.4
dihedral angle violations >5°	1.1 ± 0.9
root-mean-square deviation (rmsd) from experimental restraints	
distance (NOE and hydrogen bond) restraints (Å)	0.040 ± 0.002
dihedral angle restraints (deg)	0.9 ± 0.1
rmsd from idealized geometry	
bonds (Å)	0.0053 ± 0.0001
angles (deg)	0.63 ± 0.01
impropers (deg)	1.75 ± 0.06
rmsd of residues 811−901 from mean coordinates	
backbone atoms (N, Ca, C′) (Å)	0.33 ± 0.08
heavy atoms (Å)	0.73 ± 0.06
distribution of Φ and Ψ dihedral angles of residues 811−901 in the Ramachandran plot[56] (%)	
most favored regions	83.6
additional allowed regions	16.1
generously allowed regions	0.1
disallowed regions	0.3

Results

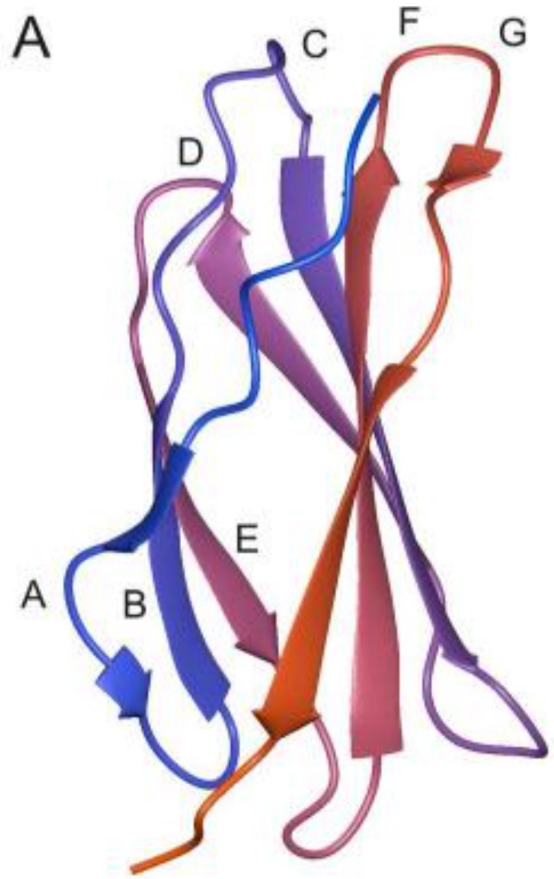

Figure 3. Solution structure of 3FN3. (A) Ribbon model of 3FN3 (residues 811−901). The color changes smoothly from blue at the N-terminus to red at the C-terminus, and the individual β-strands are labeled. (B) Twenty-five superimposed backbone traces of 3FN3. The coloring scheme and orientation are the same as in panel A. (C and D) Hydrophobic core in 3FN3. To illustrate packing at the interface between the two β-sheets, the side chains of buried residues are shown in a space filling representation and are colored as in panels A and B. The backbone traces are colored gray. The orientation in panel C is the same as in panels A and B, and the view in D is related by a 180° rotation around the vertical axis.

Results

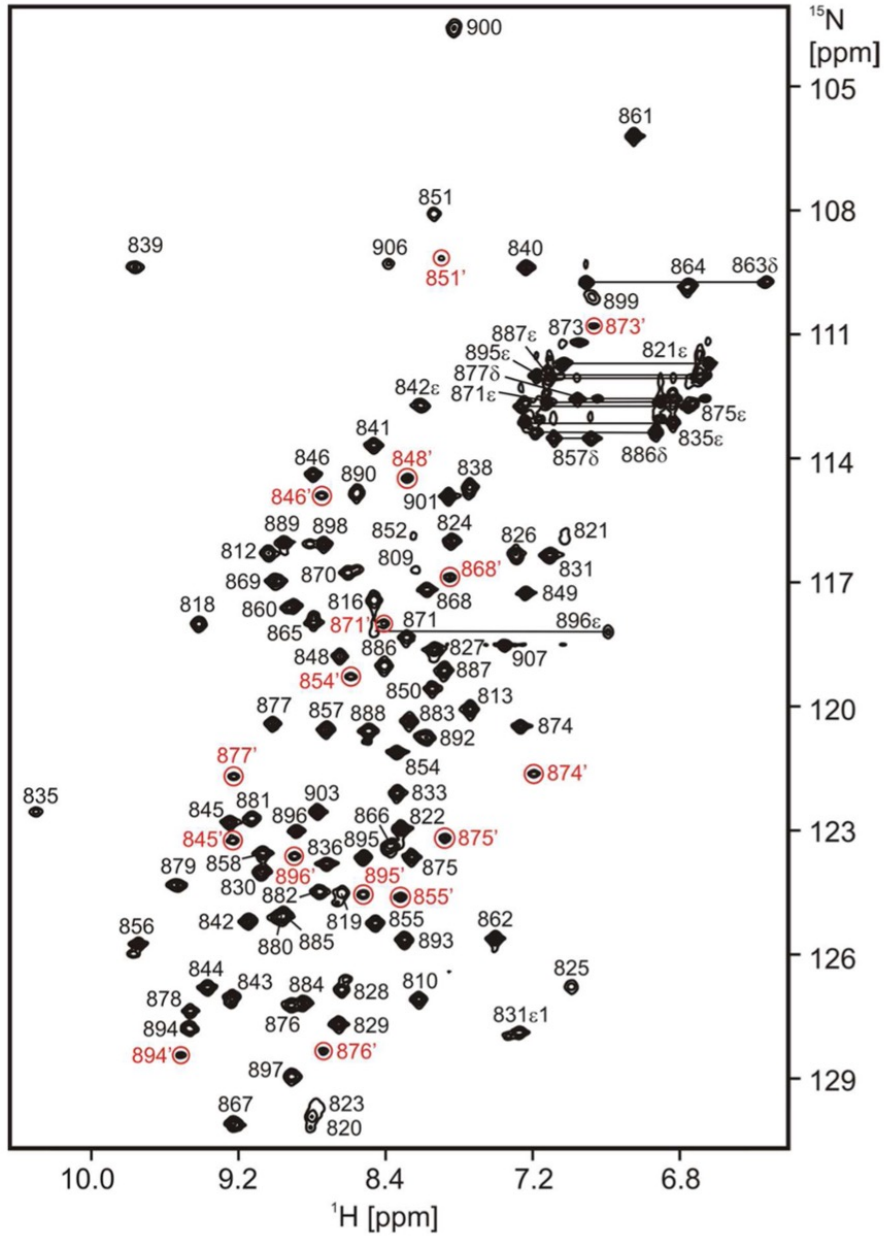

Figure 2. 2D 1H−15N HSQC spectrum of 3FN3. The assignments are indicated. Cross-peaks from the minor species that do not adjoin their respective major peaks are highlighted in red and denoted by an apostrophe. Signals from T825 and R842ε are aliased from 97.76 and 83.67 ppm, respectively.

Cross peaks between H and N15 atoms that are directly bonded

Results

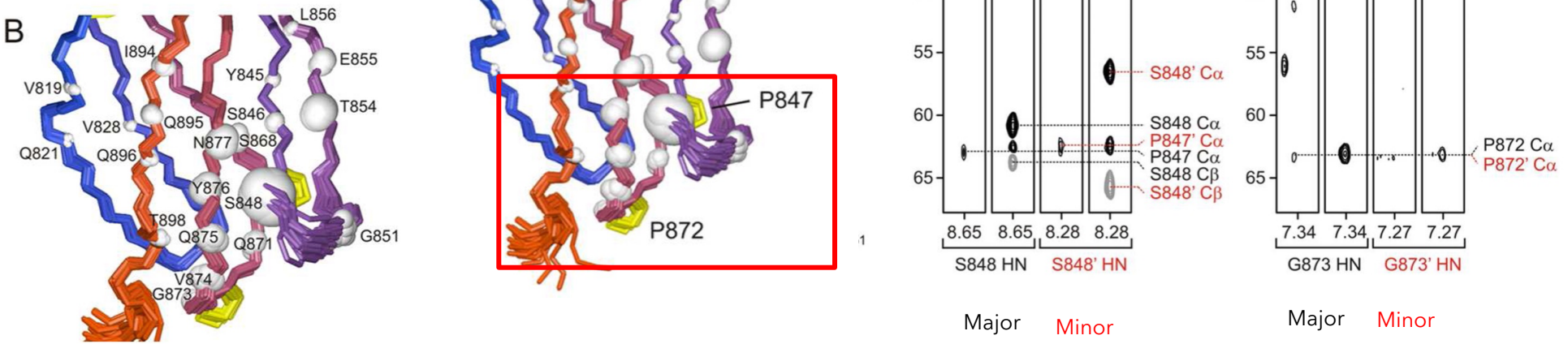

Cis-trans isomerization of S848-P847 peptide bond

Figure 6. Conformational heterogeneity in 3FN3. (A) Backbone amide chemical shift heterogeneity mapped onto the 3D structure of 3FN3. The backbone amide nitrogen of each residue with a minor cross-peak in the 2D 1H−15N HSQC spectrum (Figure 2) is displayed as a white sphere. The volume of the sphere is proportional to the chemical shift difference between the cross-peaks of the major and minor form. The backbone traces are colored as in panels A and B of Figure 3. Proline side chains are colored yellow and labeled to help visualize their positions relative to the residues whose chemical shifts differ between the two forms. P902, which is located in the dynamic C-terminal tail, is not shown. The view is related to the orientation in Figure 3A−Cbya40° rotation around the vertical axis. (B) Close-up view with the residues labeled. (C and D) 13C chemical shifts of P847 and P872, respectively, as observed in the 3D C(CO)NH and HNCACB spectra. The left two strips in each panel are for the major conformer, and the right two strips are for the minor conformer. Positive contour levels are colored black and negative levels gray. The chemical shift assignments for the minor conformer are denoted with an apostrophe and are colored red, and the assignments for the major conformer are colored black.

Results

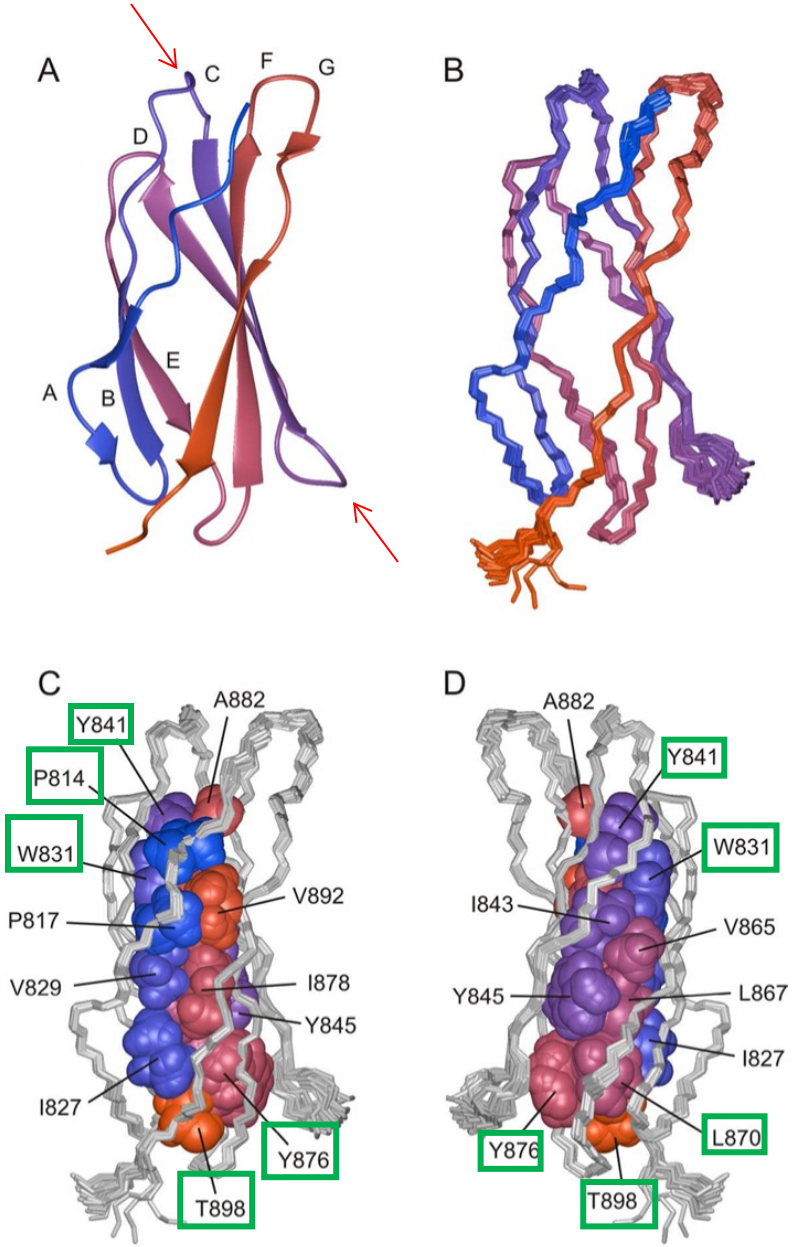

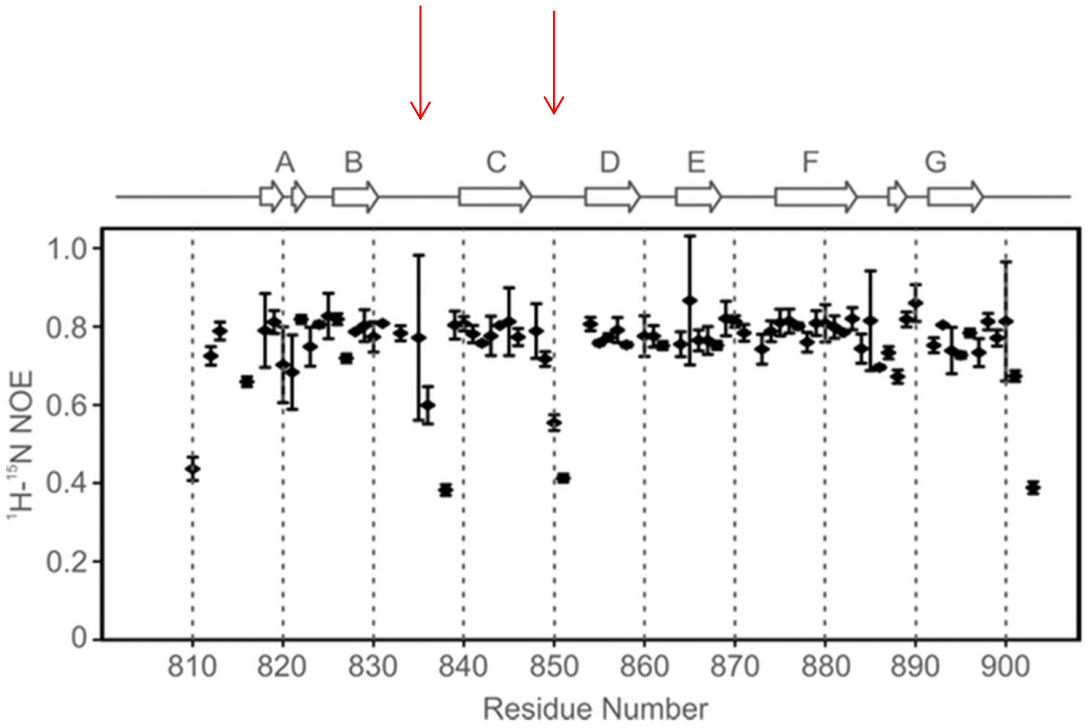

Figure 5. Backbone amide dynamics in 3FN3: 1H−15N NOE data. The secondary structure of 3FN3 is outlined at the top. The 1H−15N NOE values for D905, g906, and t907 are negative and are not included in the figure.

Figure 3. Solution structure of 3FN3. (A) Ribbon model of 3FN3 (residues 811−901). The color changes smoothly from blue at the N-terminus to red at the C-terminus, and the individual β-strands are labeled. (B) Twenty-five superimposed backbone traces of 3FN3. The coloring scheme and orientation are the same as in panel A. (C and D) Hydrophobic core in 3FN3. To illustrate packing at the interface between the two β-sheets, the side chains of buried residues are shown in a space filling representation and are colored as in panels A and B. The backbone traces are colored gray. The orientation in panel C is the same as in panels A and B, and the view in D is related by a 180° rotation around the vertical axis.

Experimental Procedures

Shifting to 3FN3 and Anastellin….

- Structure determination of 3FN3
  - NMR experiments
  - Structure Calculations
- Folding/unfolding kinetics
  - Equilibration denaturation studies
  - Kinetic analysis

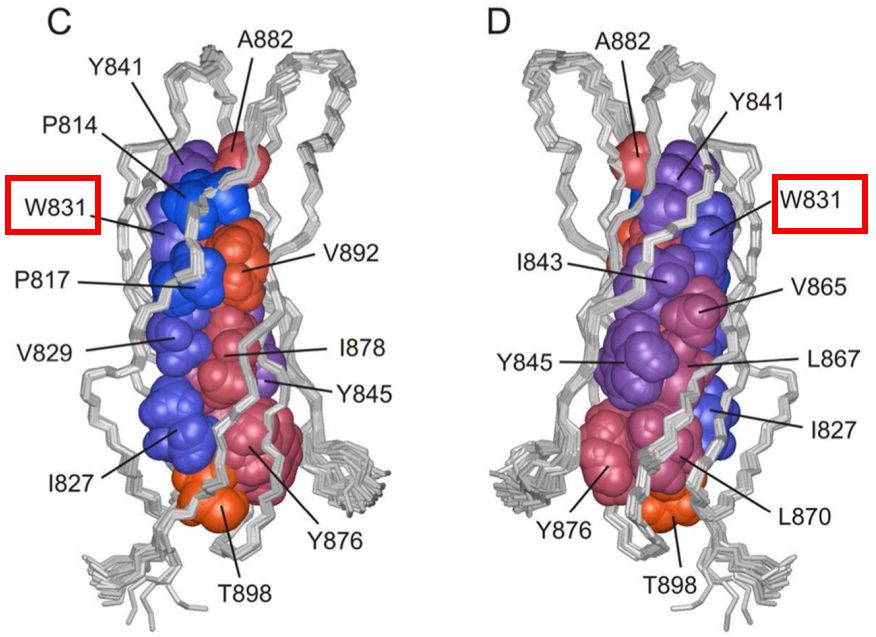

Presentation Structure

Introduction

Objectives

Experimental Procedures

Results

Overall Findings

Results

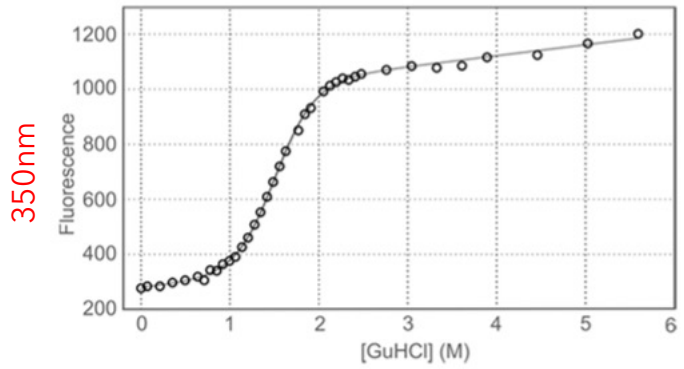

Figure 7. Equilibrium denaturation of 3FN3 in GuHCl. The black curve represents the equation fitted to the data.

JASCO FP-8200 spectrofluorometer at 24°C

- Samples equilibrated w/denaturant for 2hrs
- Average of triplicate runs
- [GuHCl] of $1.51 \pm 0.02M$
- Free energy of unfolding in presence of GuHCl $2.65 \pm 0.17\frac{kcal}{mol \cdot M}$
- Free energy of unfolding in absence of GuHCl $4.00 \pm 0.26\frac{kcal}{mol}$
- No deviation from the two forms.

$$F = [(\alpha_F + \beta_F[D]) + (\alpha_U + \beta_U[D])\exp\{\left(m[D] - \frac{[D]_{50\%}}{RT}\right\}]/[1 + \exp\left\{\frac{m[D] - [D]_{50\%}}{RT}\right\}]$$

Results

3FN3 unfolding rate= $0.057 \pm 0.0010\ s^{-1}$

Anastellin unfolding rate= $0.02\ s^{-1}$

minor

major

Solid circle = unfold

Open circle and dash = refold

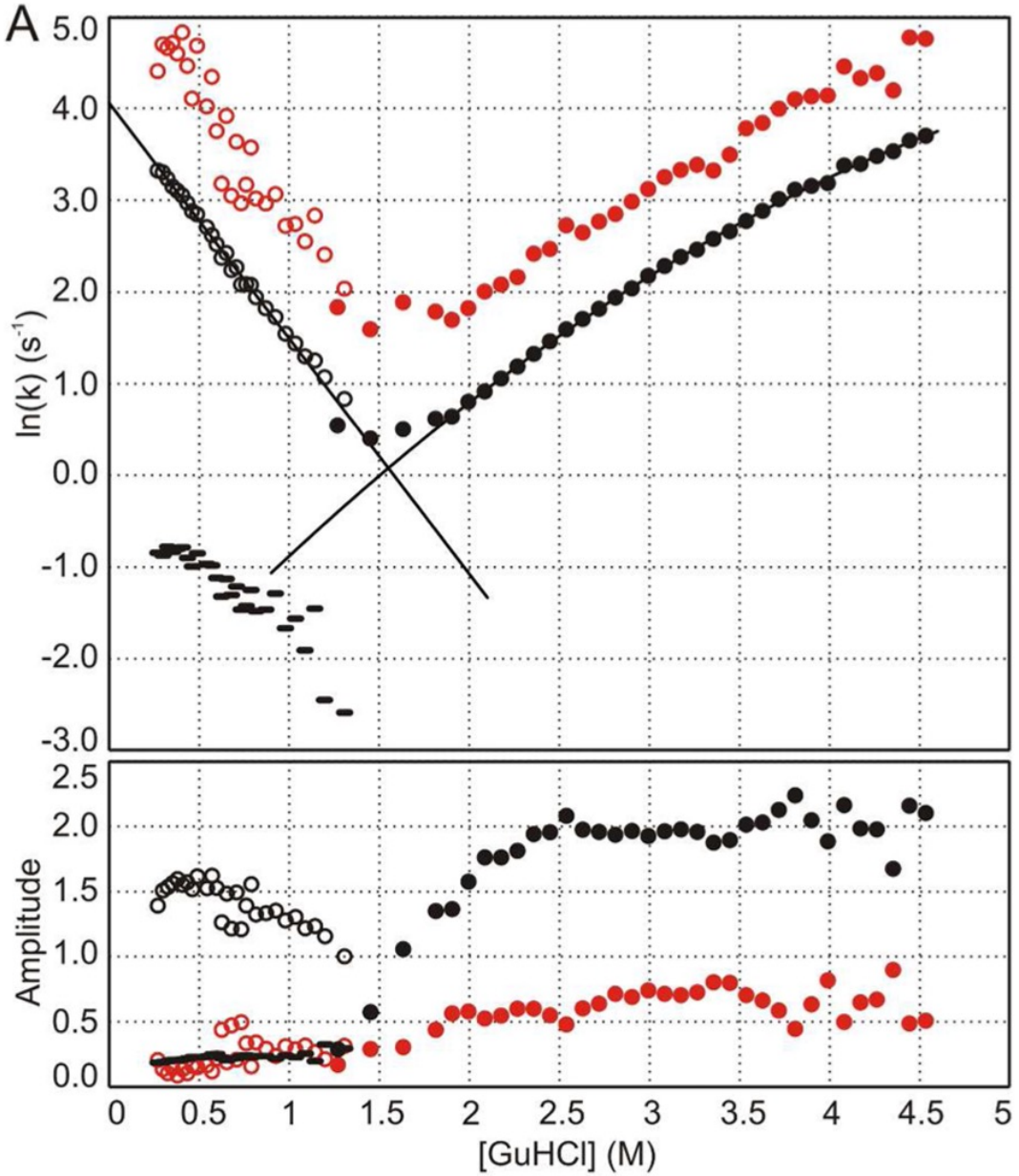

Figure 8. Kinetics of 3FN3 folding and unfolding. (A) Natural logarithm of the rate constants (top) and the amplitudes (bottom) shown as a function of GuHCl concentration for two unfolding (black and red filled circles) and three refolding (black and red empty circles and black dashes) phases. The slowest refolding phase that was detected in only a 3 min experiment is not included in the plot. The solid black lines represent the equations fitted to the data for the major unfolding and refolding phases.

Presentation Structure

Introduction
Objectives
Experimental Procedures
Results
Overall Findings

Overall Findings

3D structure determination of 3FN3

3FN3 is conformationally heterogeneous

3FN3 displays low stability and a higher unfolding rate

3FN3 has a comparable unfolding rate to the binding rate of Anastellin

Thank you

References

Ohashi, T., Augustus, A. M., and Erickson, H. P. (2009) Transient opening of fibronectin type III (FNIII) domains: the interaction of the third FNIII domains of FN with anastellin. Biochemistry 48, 4189−419

Mosher, D. F. (1989) Fibronectin, Academic Press, New York.

Briknarova, K., Åkerman, M. E., Hoyt, D. W., Ruoslahti, E., and Ely, K. R. (2003) Anastellin, an FN3 fragment with fibronectin polymerization activity, resembles amyloid fibril precursors. J. Mol. Biol. 332, 205−215.

Stine, J. M., Sun, Y., Armstrong, G., Bowler, B. E., & Briknarová, K. (2015). Structure and unfolding of the third type III domain from human fibronectin. *Biochemistry*, *54*(44), 6724–6733.

Kaur, J., and Reinhardt, D. P. (2015) Chapter 3 - Extracellular Matrix (ECM) Molecules. in *Stem Cell Biology and Tissue Engineering in Dental Sciences* (Vishwakarma, A., Sharpe, P., Shi, S., and Ramalingam, M. eds.), Academic Press, Boston. pp 25-45

Bradshaw, A. D. (2016) The Extracellular Matrix. in *Encyclopedia of Cell Biology* (Bradshaw, R. A., and Stahl, P. D. eds.), Academic Press, Waltham. pp 694-703

Questions?